EVOLUTION OF THE MAGNETIC ENERGY BUDGET IN AR 10486 FROM POTENTIAL AND NONLINEAR FORCE-FREE MODELS

Stéphane Régnier[1], Bernhard Fleck[1], Valentyna Abramenko[2], and Hong-Qi Zhang[3]

[1]ESA Research and Support Scientific Department, Keplerlaan 1, 2201 AZ Noordwijk, The Netherlands
[2]Big Bear Solar Observatory, 40386 North Shore Lane, 92314 Big Bear City, CA, USA
[3]National Astronomical Observatories, Chinese Academy of Sciences, Beijing 100012, China

ABSTRACT

Over two weeks in October/November 2003, the Sun featured unusually strong activity, with three large sunspot groups (including the largest one of this solar cycle), twelve X-class flares (including the strongest ever recorded), numerous halo coronal mass ejections (two with near-recorded speeds) and two significant proton storms. Eight of he twelve X-class flares originated from active region AR 10486. To understand the reasons of this peculiar activity, we investigate the evolution of the coronal magnetic field configuration as well as the energetics of AR 10486 before and after the X17.2 flare on October 28. To determine the coronal mangetic fields, we use potential and nonlinear force-free reconstruction techniques using line-of-sight (SOHO/MDI) and vector (MSO/IVM, HSOS/MCST, NJIT/BBSO) magnetograms on the photosphere as boundary conditions. We identify the source region of the flare as related to the existence of a null point or separator field line evidenced in a reversed-Y magnetic configuration. From the 3D configurations we derive the magnetic energy budget which can be released during the impulsive phase of the flare. The estimated free magnetic energy is enough to produce an X-class flare. The continuous evolution of the magnetic energy derived from the potential field extrapolations indicates that the flare does not modify the distribution of magnetic field on the photosphere. We also study the distribution of energy before and after the flare using different magnetic field measurements.

Key words: Sun: magnetic fields; Sun: CME.

1. INTRODUCTION

In the solar corona, the magnetic field plays the most important role (plasma $\beta < 1$). Therefore the first step to understand the evolution of active regions, eruptive events and all other phenomena occuring in the corona is to determine how the magnetic field is structured. As the measurement of the full magnetic vector in the corona is still challenging, one can use methods to extrapolate the magnetic field into the corona starting from photospheric magnetic field measurements at the bottom boundary. The potential field represents the minimum magnetic energy field and is useful to describe a rapid and/or a long-term evolution of active regions: only the line-of-sight component of the magnetic field is needed to extrapolate into the corona, and the registration of one magnetogram is fast (e.g., $<$ 1 min for a full disc SOHO/MDI magnetogram). The nonlinear force-free field assumption is currently the most advanced model to determine the 3D coronal mangetic field. This method requires the knowledge of the full magnetic field vector in the photosphere. The observations of vector magnetograms still suffer from a poor time cadence (only a few per day) which limits our investigation on the evolution of active regions. The nonlinear force-free method allows us to estimate the free magnetic energy budget (difference between the magnetic energy of the nonlinear force-free field and of the potential field) which determines the amount of magnetic energy that can be released during a flare. In the following, we apply both reconstruction methods (potential and nonlinear force-free) to understand the long-term evolution of an active region, the geometry and the topology of the magnetic field as well as the storage and release of magnetic energy before and after the flare.

For our study, we have chosen the active region 10486 (AR 10486) observed on October and November 2003. AR 10486 is associated with the most important flaring activity period of this solar cycle. In particular, we focus on the X17.2 flare which occurred near disc center on Oct. 28 at 11:10 UT. The eruptive event is related to an Earth-directed coronal mass ejection and a proton storm. In order to describe the evolution of AR 10486, we proceed in two steps: (i) the continuous long term evolution is anal-

ysed using line-of-sight magnetograms and the associated potential field reconstructions; (ii) the evolution of the nonlinear force-free field before and after the flare is studied using 3 different observations of the photospheric vector magnetic fields at three different times (two before and one after the flare).

2. DATASETS

2.1. Line-of-sight magnetograms

To compute the potential field of AR 0486 only the vertical component of the magnetic field at the photospheric level is required. We perform this analysis using a time series of line-of-sight magnetic field measurements recorded by SOHO/MDI (Scherrer et al., 1995). We use a time series of 96 minute cadence magnetograms from October 27 to October 29. In order to make a reliable comparison of the relevant quantities, the field-of-view is the same for the entire time series and large enough to include the entire active region during all days. The magnetograms are projected onto the disc-center heliographic frame.

2.2. Vector magnetograms

It is still difficult to find vector magnetic field measurements with a good time coverage (only few per day). For the present study we have decided to combine different instruments to obtain information on the evolution of the nonlinear force-free field before and after the X17.2 flare. To our knowledge, only photospheric observations are available for the 27th at 18:36 UT from MSO/IVM (Mickey et al., 1996), for the 28th from HSOS/MCST (Deng et al., 1997) at 02:42 UT and from NJIT/BBSO (see e.g. Spirock et al., 2002) at 17:15 UT. IVM, MCST and BBSO provide the measurements in the Fe I line at 630.25 nm, the Fe I line at 532.4 nm and the Ca I line at 610.3 nm respectively. We extend the field-of-view of each instrument by adding SOHO/MDI observations around the vector field images. We then have the same field-of-view for each observation. We transform the images into the disc-center heliographic frame. As the magnetic field is measured in a different way for each instrument, the calibration is also different and can lead to discrepancies between observations. In order to deal with the calibration problem, we have decided to cross-calibrate the composite magnetograms using SOHO/MDI data registered at the same time as the associated vector field.

3. 3D MAGNETIC CONFIGURATIONS FROM POTENTIAL FIELD

The potential field reconstructions are used to follow the evolution in time of the magnetic energy

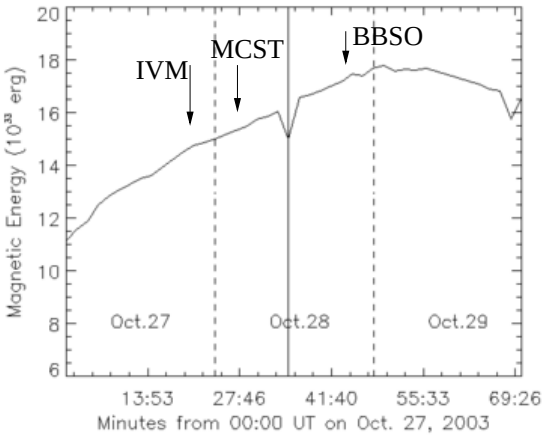

Figure 1. Time evolution of the potential field magnetic energy using a time series of 96 minute cadence SOHO/MDI magnetograms as boundary conditions. The dashed lines are separations between two consecutive days. The solid line marks the time of the X17.2 flare on Oct 28.

of AR 10486. In Régnier & Fleck (2004), we described the time evolution of AR 10486 using both 96 minute cadence and 1 minute cadence time series of SOHO/MDI magnetograms. We noticed that the source of the flare can be identified by looking at the changes observed in the vertical component of the magnetic field: a disturbance (or two ribbon flare) seen as parasitic measurements in the SOHO/MDI magnetograms propagates away from the flare site. In Figure 1, the evolution of the potential field magnetic energy is computed for the 96 minute cadence time series. We note that the magnetic energy is increasing during the first two days from Oct. 27 at 00:00 UT to Oct. 29 at 01:00 UT. The magnetic energy increases from 11 10^{33} erg to 17.6 10^{33} erg in two days which corresponds to a factor of 1.6. The potential field magnetic energy is a minimum of magnetic energy that a magnetic configuration can have with the prescribed boundary conditions, and a potential field configuration cannot store magnetic energy due to twist or writhe of flux tubes. Therefore the evolution of the potential field magnetic energy is mostly due to the increase of the photospheric unsigned flux caused by flux emergence in existing or newly emerged polarities.

4. 3D MAGNETIC CONFIGURATIONS FROM NONLINEAR FORCE-FREE FIELD

We now discuss the magnetic field topology and the magnetic energy of AR 10486 at different times before and after the flare and assuming that the magnetic field is well described by a nonlinear force-free

field. We used the vector potential Grad-Rubin reconstruction technique which uses the vertical component of the magnetic field as well as the distribution of $\alpha = \frac{J_z}{B_z}$ in only one polarity as photospheric boundary conditions (see Amari et al., 1997, 1999). Following Sakurai (1989), this method corresponds to a mathematically well-posed boundary value problem.

We compute the nonlinear force-free field for the three vector magnetograms in the same coronal volume. In Figures 2–4 we plot few characteristic field lines in the vicinity of the flare site. The background image is the vertical component of the magnetic field. We notice that the configuration is similar for magnetic configurations before the flare (sides view in Fig. 2 and Fig. 3), and the connectivity of the field lines is strongly modified after the flare (Fig. 4). We also note that the vertical component of the magnetic field is not modified during the event.

One important value to characterize the magnetic configurations is the magnetic energy. From the nonlinear force-free extrapolations, we can compute the magnetic energy of the nonlinear force-free field (E_{nlff}) and the free magnetic energy budget ($E_{free} = E_{nlff} - E_{pot}$) as well as the percentage of free energy inside the nonlinear force-free configurations. The potential field magnetic energy (E_{pot}) is computed using the vertical component of the magnetic field given by the different vector magnetograms. The values are summarized in Table 1. The values of E_{nlff} are increasing during the evolution of AR 10486. The evolution of E_{nlff} is comparable to the evolution of the potential field magnetic energy (see Section 3). The slope of the E_{nlff} evolution is steeper before the flare than during the period including the flare. This indicates a release of energy during the X17.2 flare as expected. This slope of E_{nlff} before the flare is also steeper than the slope of E_{pot} which can indicate that the emergence of flux through the photosphere is also associated with the emergence of twisted flux bundles. We do not observe a decrease of the nonlinear force-free magnetic energy due to the continuous injection of magnetic energy in the magnetic configuration as evidenced by the potential field reconstructions (see Section 3). Due to the lack of data close in time to the flare, it is difficult to draw any conclusions about the change of free energy before or during the flare (MCST magnetogram).

Table 1. The magnetic energy of the nonlinear force-free configurations, the free magnetic energy budget and the percentage of free energy in the nonlinear force-free configurations for the three different vector magnetograms before and after the X17.2 flare which occurred on Oct. 28 at 11:10 UT.

	E_{nlff} (erg)	E_{free} (erg)	% of E_{nlff}
IVM Oct. 27 at 18:36 UT	$7.05\ 10^{33}$	$4.67\ 10^{32}$	6.6%
MCST Oct. 28 at 02:42 UT	$9.22\ 10^{33}$	$1.93\ 10^{32}$	2.1%
BBSO Oct 28 at 17:15 UT	$1.03\ 10^{34}$	$8.02\ 10^{32}$	7.7%

5. DISCUSSION AND CONCLUSIONS

Even if the physical meaning of the potential field approximation is restricted, we have shown that the study of the long-term evolution of the potential field energy is useful to understand the nature of an active region. AR 10486 shows a continuous injection of magnetic flux through the photosphere. In addition nonlinear force-free computations (often time-consuming) are needed to know the geometry, the topology and the connectivity of the magnetic field. AR 10486 exhibits a reversed-Y structure at the flare site. Moreover, the free magnetic energy budget can be derived. AR 10486 contains a large amount of free energy sufficient to trigger a large flare, and the amount of free energy remains the same before and after the flare due to the continuous emergence of magnetic flux.

ACKNOWLEDGMENTS

S. R.'s research is funded by the European Commission's Human Potential Programme throught the European Solar Magnetism Network (contract HPRN-CT-2002-00313).

REFERENCES

Amari, T., Aly, J. J., Luciani, J. F., Boulmezaoud, T. Z., Mikic, Z. 1997, Solar Phys., 174, 129

Amari, T., Boulmezaoud, T. Z., Mikic, Z. 1999, A&A, 350, 1051

Deng, Y., Ai, G., Wang, J., Song, G., Zhang, B., Ye, X. 1997, Solar Phys., 173, 207

Mickey, D. L., Canfield, R. C., Labonte, B. J., Leka, K. D., Waterson, M. F., Weber, H. M. 1996, Solar Phys., 168, 229

Régnier, S., Fleck, B. 2004, in ESA SP-575: SOHO 15 Coronal Heating, p.519

Sakurai, T. 1989, Space Science Reviews, 51, 11

Scherrer, P. H., et al. 1995, Solar Phys., 162, 129

Spirock, T. J., Yurchyshyn, V. B., Wang, H. 2002, ApJ, 572, 1072

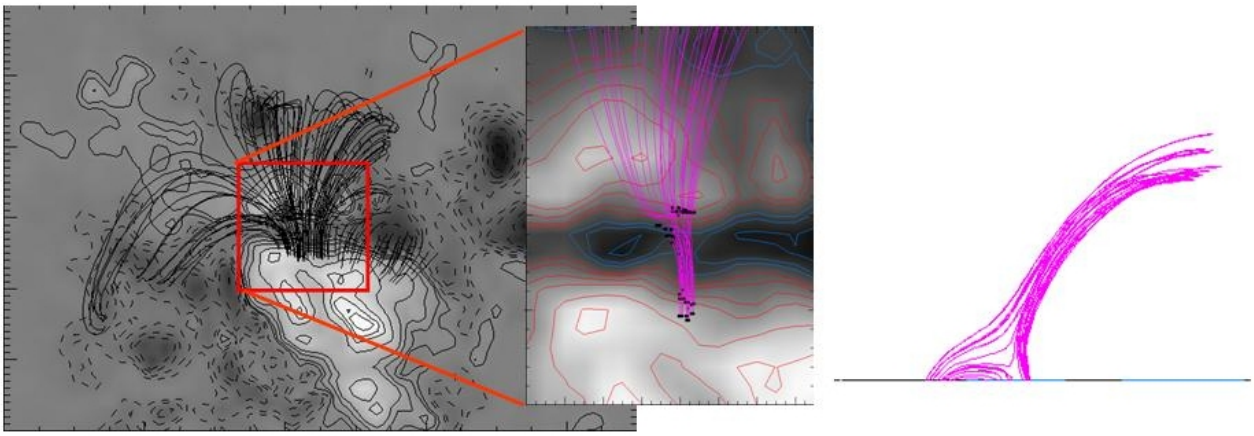

Figure 2. Nonlinear force-free magnetic field from IVM vector magnetogram at 18:36 UT on Oct. 27. The images on the left are two top views of the entire active region and of the flare site. The right image is a side view at the flare site. The magnetic configuration exhibit a reversed-Y shape topology.

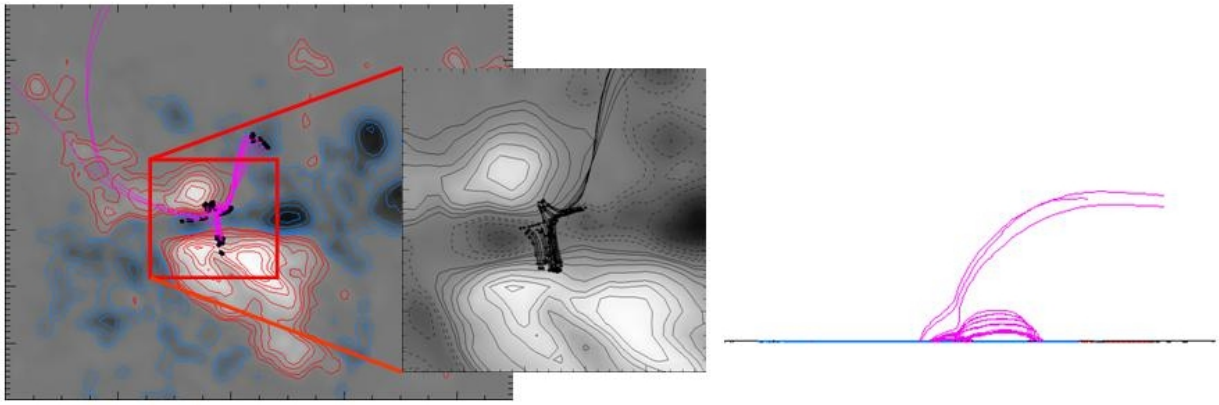

Figure 3. Nonlinear force-free magnetic field from MCST vector magnetogram at 02:42 UT on Oct. 28. Images: same as described in Fig. 2. The same reversed-Y shape as in Fig. 2 is observed.

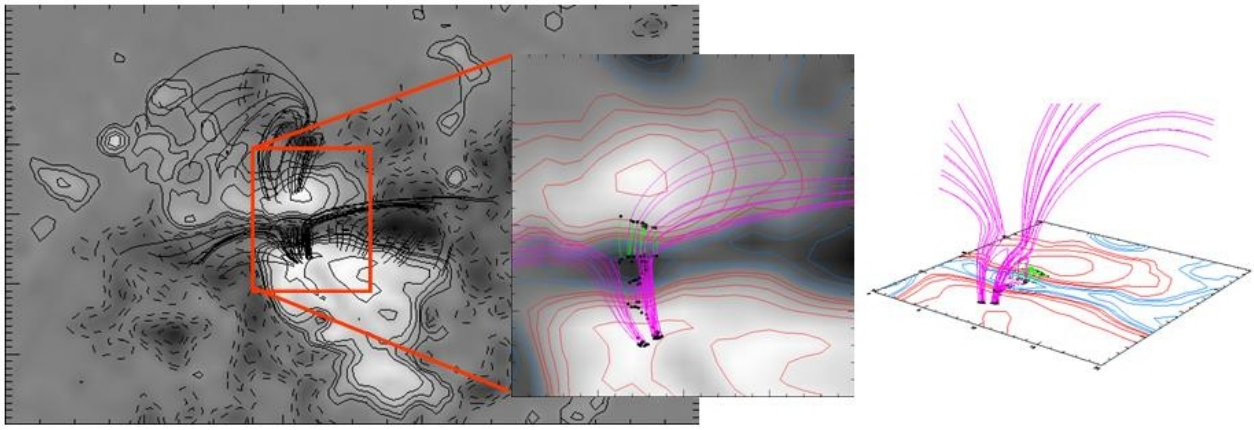

Figure 4. Nonlinear force-free magnetic field from BBSO vector magnetogram at 17:15 UT on Oct. 28. Same figures as for Fig. 2. The topology near the flare site is still complex but the connectivity of the field lines is obviously completely different.